Supplementary Materials for

Edge Polarization Topology Integrated with Sliding Ferroelectricity in Moiré System

Wen-Cheng Fan[1]†, Zhao Guan[1]†, Lu-Qi Wei[1]†, Hao-Wen Xu[1]†, Wen-Yi Tong[1]†, Ming Tian[2], Neng Wan[2], Cheng-Shi Yao[1], Jun-Ding Zheng[1], Ya-Qiong Wang[1], Bin-Bin Chen[1], Ping-Hua Xiang[1,3*], Ni Zhong[1,3*] & Chun-Gang Duan[1,3*]

[1] Key Laboratory of Polar Materials and Devices, Ministry of Education & Shanghai Center of Brain-inspired Intelligent Materials and Devices, East China Normal University, Shanghai, 200241, China.

[2] Key Laboratory of MEMS of Ministry of Education, School of Integrated Circuits, Southeast University, Nanjing, China

[3] Collaborative Innovation Center of Extreme Optics, Shanxi University, Taiyuan, Shanxi, 030006, China.

*Corresponding author. Email: nzhong@ee.ecnu.edu.cn (N. Z.), phxiang@ee.ecnu.edu.cn (P.H.X.), cgduan@clpm.ecnu.edu.cn (C.G.D.)

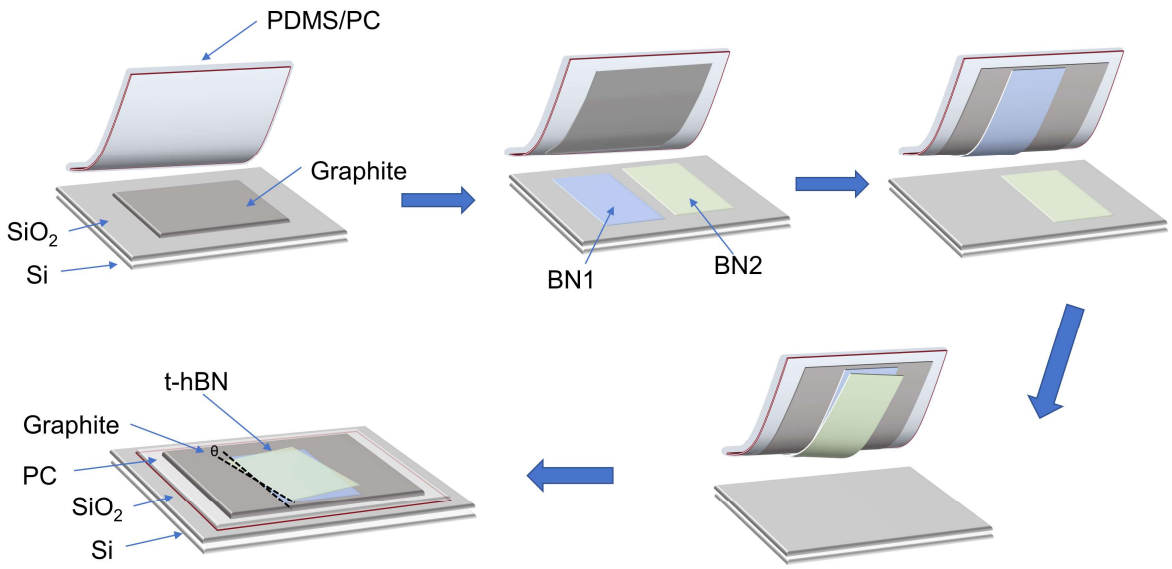

Fig. S1. Flowchart of the construction process for t-BN. The t-BN sample was constructed using the tear-and-rotate technique with PDMS/PS to transfer BN.

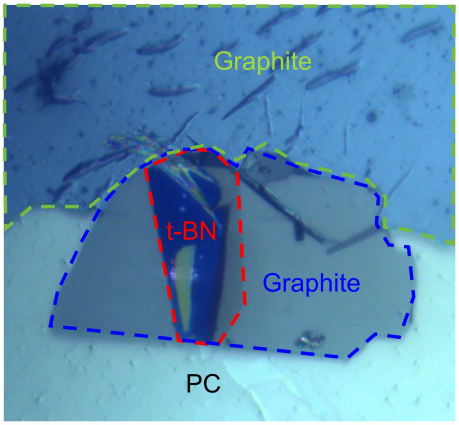

Fig. S2. Optical image of the t-BN sample.

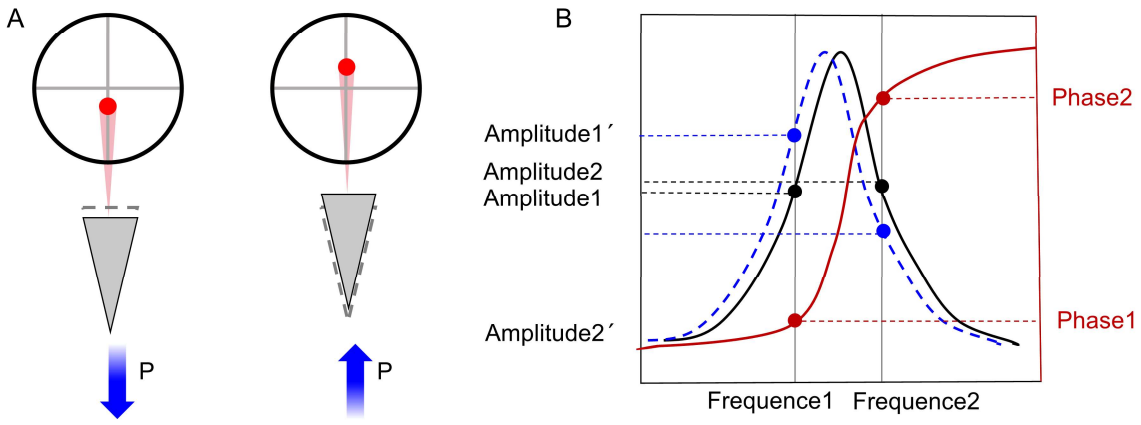

Fig. S3. Principle of PFM. (*44*, *45*) (A) Schematic diagram of V-PFM. When the conductive probe with alternating current interacts with the sample, it can induce periodic oscillations of expansion and contraction in ferroelectric systems due to the converse piezoelectric effect. In this mode, it collects domain information perpendicular to the sample surface, which is commonly referred to as vertical PFM (V-PFM). (B) Schematic diagram of Dual AC Resonance-Tracking (DART) PFM. The scanning process concurrently tracks two distinct resonant frequencies of the tip, channeling the piezoelectric signals measured at these frequencies to separate lock-in amplifiers for processing. This setup facilitates amplitude and phase measurements at different frequencies. As the contact forces between the probe and sample lead to continuous changes in the resonant frequency, Amplitude 1 shifts to Amplitude 1' and Amplitude 2 shifts to Amplitude 2'. By maintaining a constant difference between these two amplitudes, dual-frequency resonance tracking is achieved. This method prevents signal cross-talk caused by resonance frequency shifts, ensuring more stable piezoelectric signals. Additionally, it offers enhanced sensitivity, enabling the detection of weaker piezoelectric signals, such as those in low-dimensional ferroelectric materials.

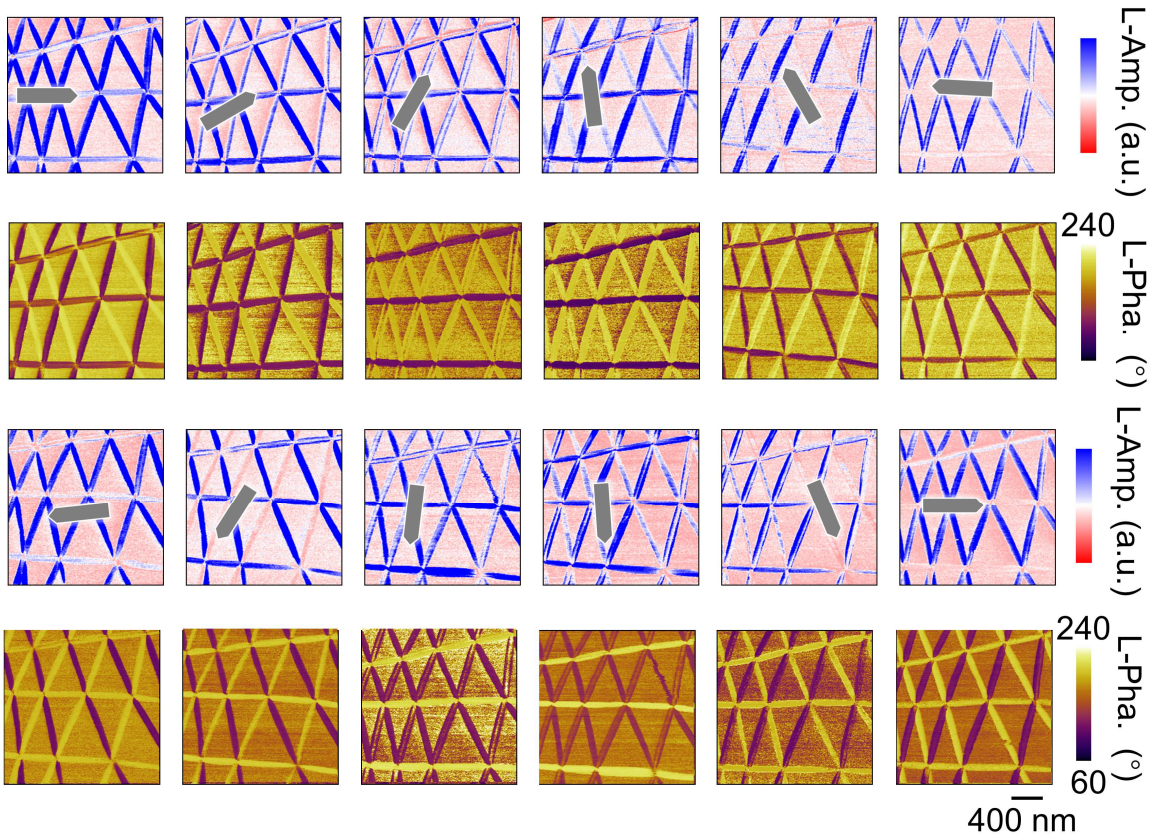

Fig. S4. L-PFM tests were performed by rotating the sample every 30° within 0-360°. From up to down are the L-Amp. and L-Pha. images, respectively.

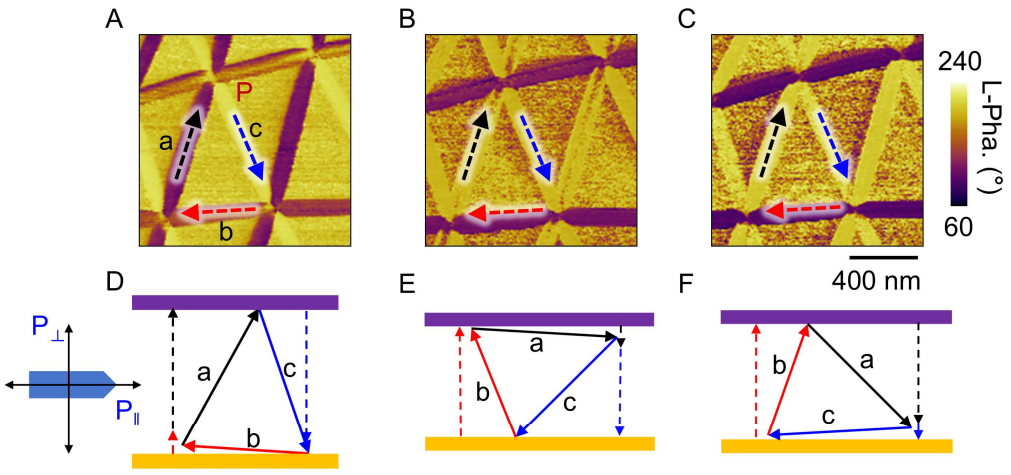

Fig. S5. IP polarization vector decomposition. (A-C) L-PFM phase images with the cantilever beam parallel to sides a, b, and c, respectively. (D-F) IP polarization at the edge is vectorially decomposed along the cantilever.

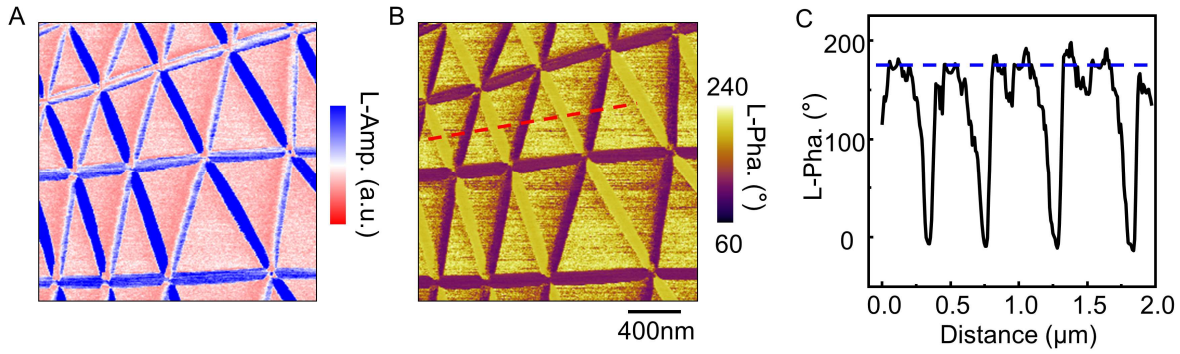

Fig. S6. IP PFM characterization of t-BN moiré patterns. (A) L-PFM amplitude and (B) phase images of t-BN. (C) Phase profile extracted along the red curve in figure B.

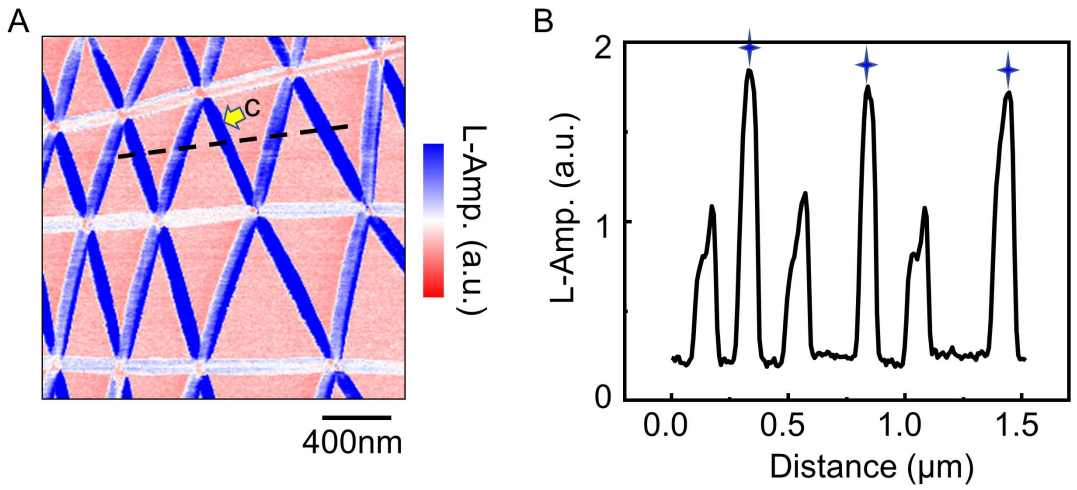

Fig. S7. IP amplitude response and magnitude. (A) L-PFM amplitude image. **(**B) Amplitude profile extracted along the black dashed line in figure A.

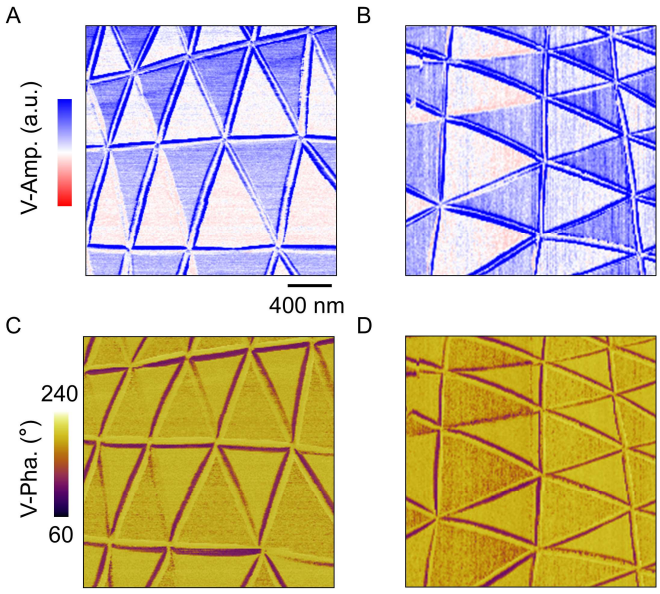

Fig. S8. V-PFM characterization after 90° rotation of the sample. (A) V-Amp. and (C) V-Pha. images of t-BN at 0°. (A) V-Amp. and (C) V-Pha. images of t-BN at 90°.

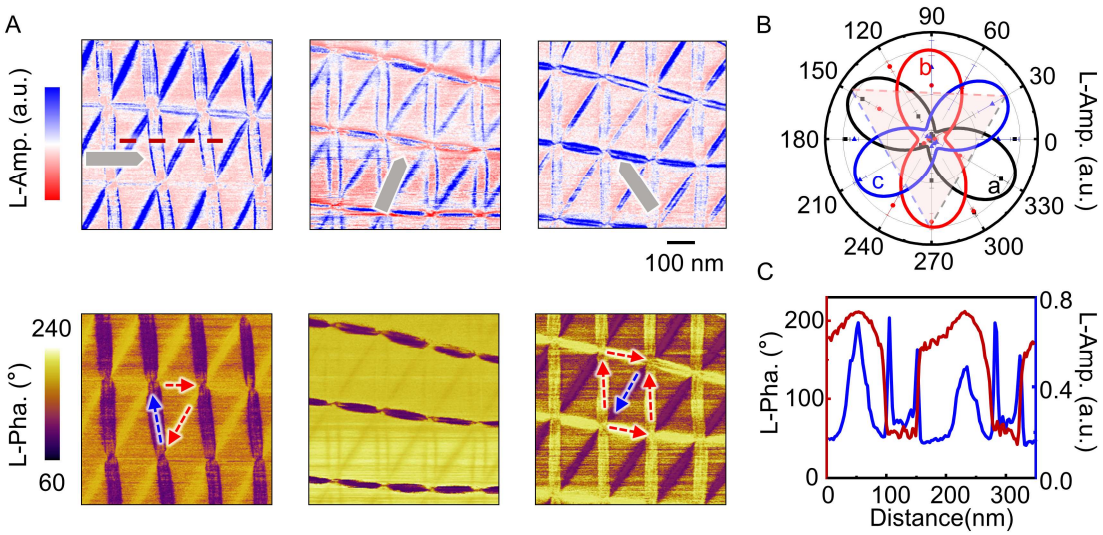

Fig. S9. IP merons and anti-merons in t-WSe_2. (A) L-Amp. and L-Pha. signals of t-WSe_2 with the tip perpendicular to the three sides of triangular moirés. There is a significant amplitude response at the edge, with no amplitude response inside the triangles, indicating that IP polarization is only distributed at the edge, and exhibits a head-to-tail connected vortex and anti-vortex topological structure. (B) Polar plots of the L-amp. obtained from images at different tip-sample angles (from 0° to 360° with a step of 30°). The amplitude intensity was extracted and normalized, showing that the IP polarization is parallel to the edge and aligned with the edge length, consistent with results of t-BN. (C) L-Amp. and L-Pha. profiles extracted along the red dashed lines in panel (A).

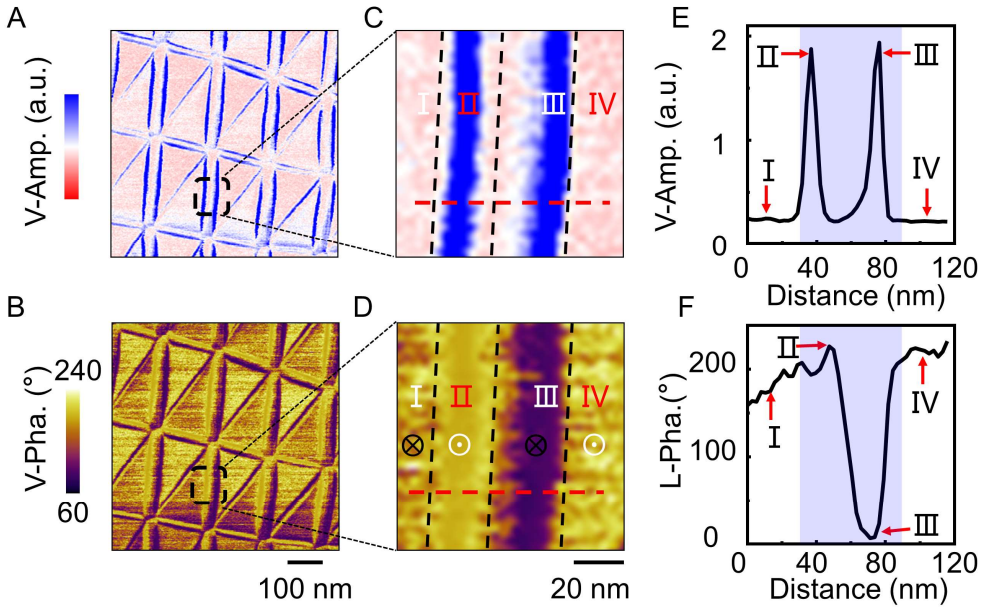

Fig. S10. OOP two-lobe edge polarization with opposite direction in t-WSe_2. (A) V-Amp and (B) V-Pha. images of the same area in Fig. S11. (C) Enlarged V-Amp. and (D) V-Pha. images of the area within the black dashed box in (A) and (B). (E) V-Amp. and (F) V-Pha. profiles extracted along the red dashed lines highlighted in (C) and (D). The OOP polarizations with opposite direction exist at the edges, with a phase difference of approximately 180°.

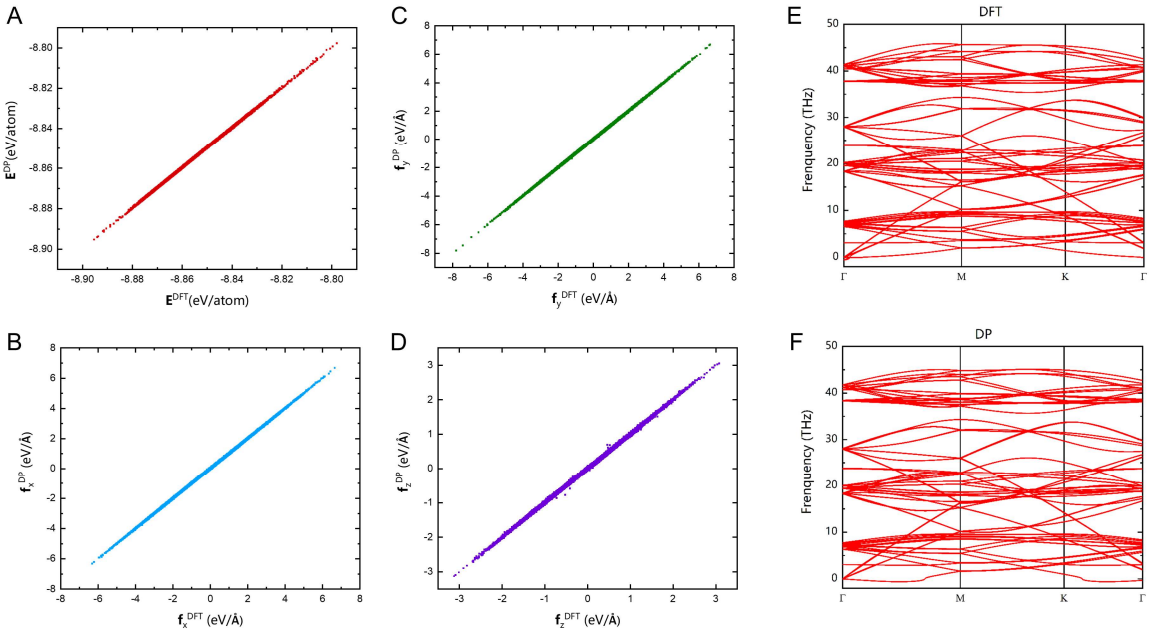

Fig. S11. Evolution of Energy/Force model. (A) Comparison of energies and atomic force components along the (B) *x*, (C) *y*, and (D) *z* axes of the DP energy model with DFT calculations for all configurations in the validation dataset. (E) The phonon spectrum of h-BN bilayer moiré structure with a twist angle of 21.79°, calculated by the DFT and (F) DP model, respectively.

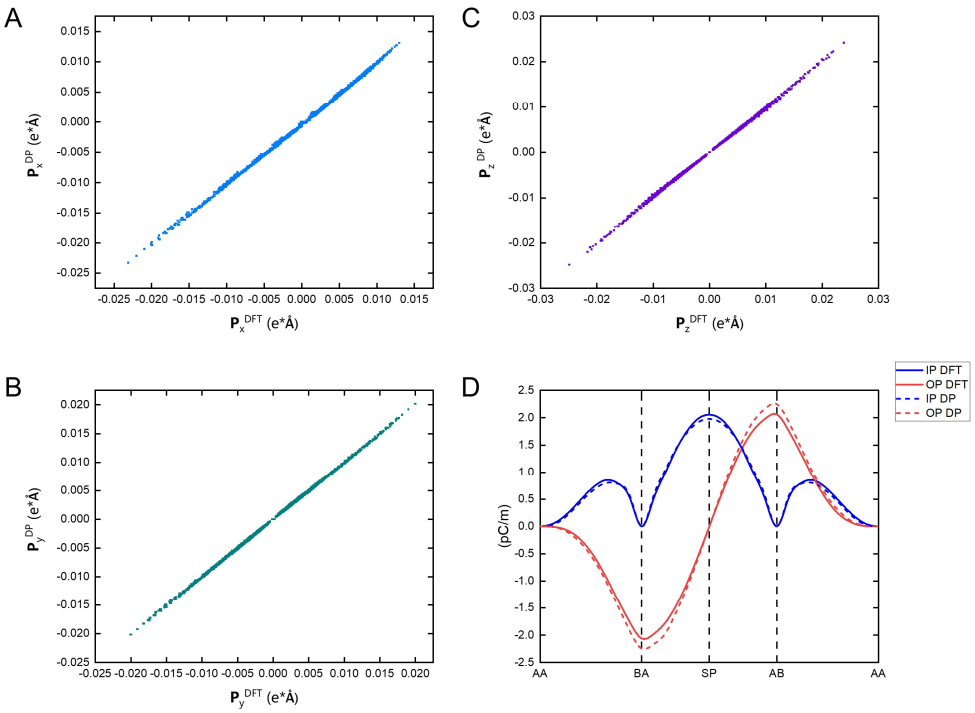

Fig. S12. Evolution of polarization model. Comparison of polarization along the (A) x, (B) y, and (C) z directions of the DP polarization model with DFT calculations for all configurations in the validation dataset. (D) Polarization calculated by DFT (solid lines) and DP model (dotted lines) for different stackings of bilayer BN. Blue lines denote IP polarization, whereas red lines indicate OOP polarization.

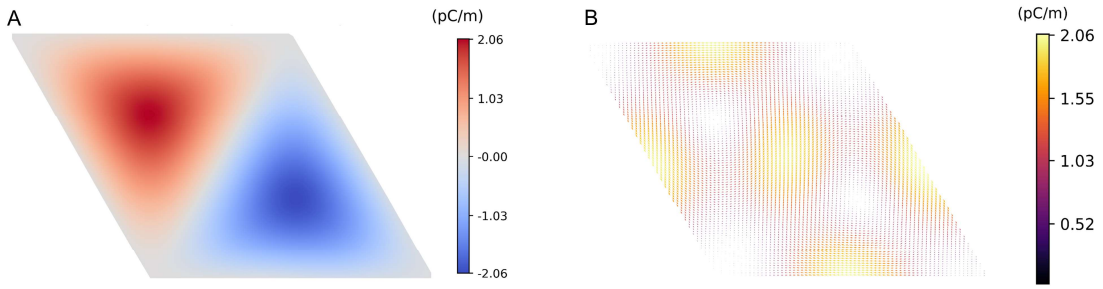

Fig. S13. (A) OOP and (B) IP polarization due to sliding ferroelectricity in unrelaxed t-BN.

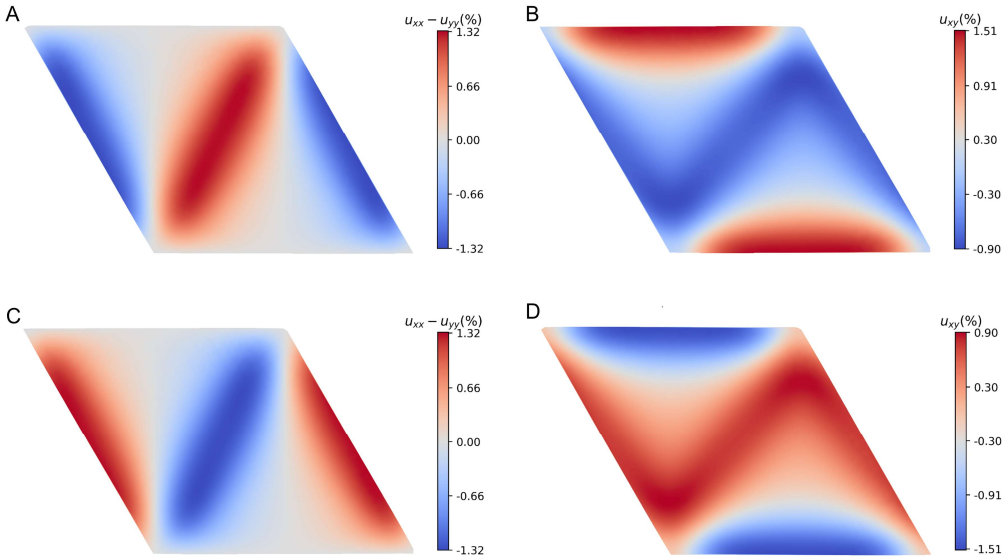

Fig. S14. Normal and shear strain field due to displacement field. (A) Normal and (B) shear strain in the upper layer due to the atomic displacement field, while (C) and (D) represent the corresponding strain fields in the bottom layer, respectively.

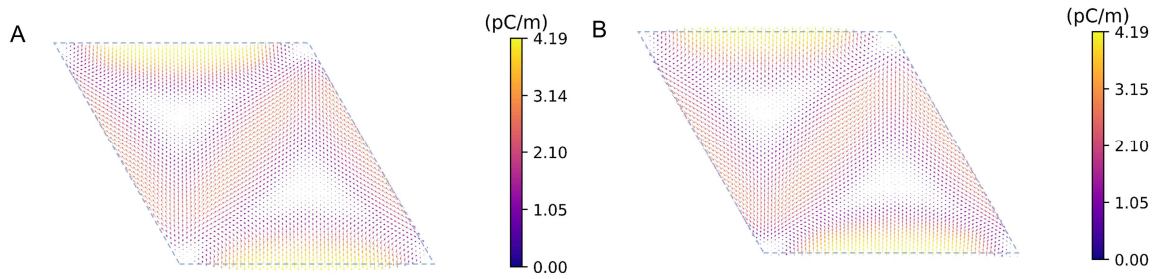

Fig. S15. IP polarization induced by piezoelectric effect. (A) Piezoelectric effect induces reversed in-plane polarization in the bottom and (B) upper layers, respectively.

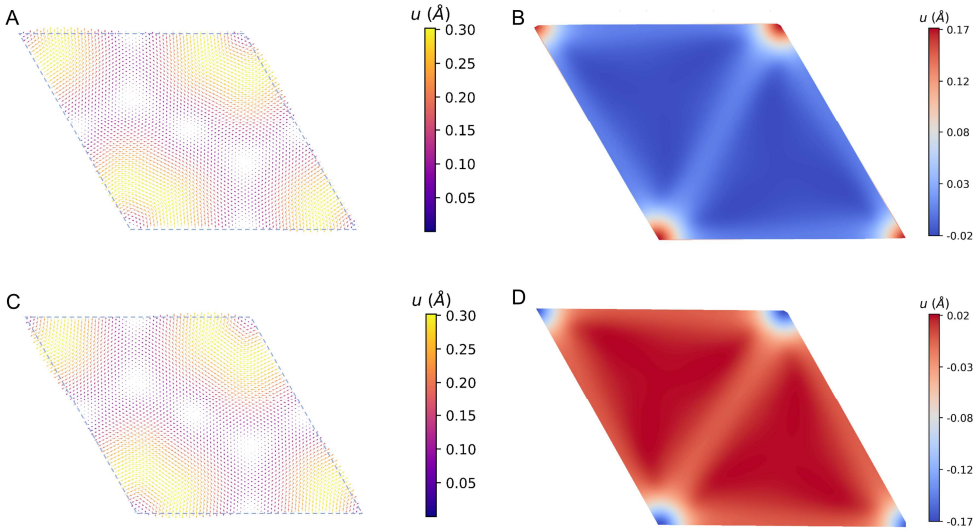

Fig. S16. IP and OP atomic displacement after structural reconstruction. (A) Upper layer of IP and (B) OOP atomic displacement after atomic reconstruction. (C) Bottom layer of IP and (D) OOP atomic displacement after atomic reconstruction.

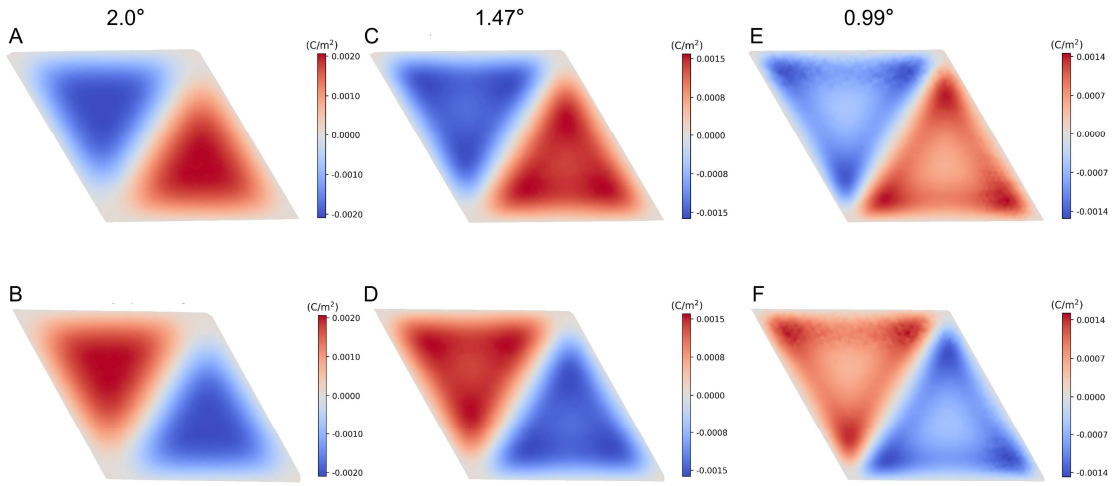

Fig. S17. Angle-dependent charge distribution arising from the induced IP polarization.

Figure (A-B) (C-D) (E-F) separately show the charge distribution when twist angle is 2.0°, 1.47°, and 0.99°. The upper and lower rows of the picture display the charge distribution of the top and bottom layers of BN, respectively.